Available online at www.sciencedirect.com
ScienceDirect
International Journal of Heat and Mass Transfer 50 (2007) 2514–2520
International Journal of HEAT and MASS TRANSFER
www.elsevier.com/locate/ijhmt

Peripheral fins for blockage robustness

Hailing Wu [a], Diana Ma [b], Massoud Kaviany [b,*]

[a] Advanced Heat Transfer LLC, Memphis, TN 38120, United States
[b] Department of Mechanical Engineering, University of Michigan, Ann Arbor, MI 48109, United States

Received 11 July 2006; received in revised form 1 December 2006

Abstract

A peripheral finned-tube, cross-flow heat exchanger (evaporator) is briefly introduced that allows for uninterrupted and effective air flow in the presence of condensate or frost. The peripheral fins are connected to tubes with radial fins and the surface areas of both radial and peripheral fins allow for surface-convection heat transfer. The peripheral fins have a staggered arrangement to allow for alternate air flow paths in the presence of a blockage. Optimized fin structure is sought using one-dimensional fin models. The peripheral fins allow for significant surface-convection by using the stagnation–flow regions as well as the boundary–layer break ups. The CFD results show that the peripheral fins mitigate the pressure drop penalty due to blockages and in this regard present an advantage over the conventional fins. CFD results show that fin pitch can be optimized. The anisotropy of the peripheral fin structure may also allow for easy drainage of the condensate along the tubes when tubes are along gravity.

1. Introduction

Frost and condensate formation are common when moist air is cooled on cold surface below the dew point (as in evaporators). The resulting air flow blockage is undesirable in air-conditioning and refrigeration heat exchangers, because of degradation it causes air flow resistance (and to a less extent because the low conductivity of condensate/frost). This changes the balance point for the system-fan characteristic curve and reduces air flow [1]. It has been reported [2] that frost formation on a compact heat exchanger causes up to 50–70% decrease in the heat transfer and a substantial increase in the pressure drop. The condensate blockage has a similar blockage effects. Retained condensate generally causes an increase in the friction factor, especially at small fin pitch and low Reynolds numbers [3–6]. It has also been found [3] that the friction factor for a plain-fin heat exchanger under wet conditions can be up to 70% higher than that under dry conditions. Also, up to 55% decrease in heat transfer rate is found under wet condition, for a plain-fin heat exchanger with a fin pitch of 1.3 mm [3].

Extensive researches have being conducted to investigate the frost and condensate phenomena [7–9], and to develop technologies to delay frost/condensate formation and control the frost growth or condensate drainage. Typical technologies includes surface treatment (surface roughness [7], coating [8]), and electro-hydrodynamics (EHD) [9].

Here, we briefly report on a radial–peripheral fin geometry design and performance for such blockage robustness. The lateral symmetry of the existing louvered fins in conventional plain-fin heat exchangers does not allow for alternate flow paths for the distributed condensate/frost. To overcome this, the connected-pore, porous-medium fluid flow path concept is used to design a periodic structure that allows for alternative fluid flow paths and for easy drainage along a pre-designed direction [10]. We first present a one-dimensional fin analysis using a random porous-medium surface-convection correlation, to identify key fin geometric parameters. Then using CFD, the flow and heat transfer characteristic are analyzed for heat exchange with and without a frost blockage. We will demonstrate the blockage robustness of this design.

* Corresponding author. Tel.: +1 734 936 0402; fax: +1 734 647 3170.
E-mail address: kaviany@umich.edu (M. Kaviany).

0017-9310/$ - see front matter © 2007 Elsevier Ltd. All rights reserved.
doi:10.1016/j.ijheatmasstransfer.2006.12.028

Nomenclature

A	total surface area of fins in a unit cell, m^2
A_{bare}	surface area of the tube not covered by fins, m^2
$A_{k,r(p)}$	cross-sectional area of conduction of a radial or peripheral fin, m^2
$A_{r(p)}$	surface area of a radial or peripheral fin, m^2
D_i	tube inner diameter, m
D_o	tube outer diameter, m
D_c	outer diameter of the fin collar, m
D_p	particle diameter, m
h_i	tube-side heat transfer coefficient, $W/(m^2\,K)$
k	thermal conductivity, W/(m K)
$L_{r(p)}$	length of a radial or peripheral fin, m
Nu	Nusselt number, –
P_f	fin pitch, or fin width, m
Pr	Prandtl number, –
$P_{r(p)}$	fin perimeter of a radial or peripheral fin, m^2
$P_{t,x}$	tube pitch in the x direction (stream-wise), m
$P_{t,y}$	tube pitch in the y direction (span-wise), m
Re	Reynolds number, –
$R_{r(p)}$	convection heat transfer resistance, K/W
T	temperature, K
U_f	velocity, m/s
V	total volume within a unit cell (both fluid and solid), m^3
V_s	volume of the solid fins within a unit cell, m^3
x, y, z	coordinate axes, m
δ_f	fin thickness, m
ε	porosity, –
ν_f	kinematic viscosity, m/s^2
δ	tube thickness, m
θ	excess temperature compared to ambient fluid temperature, K

Subscripts

b	tube base
bare	area of tube not covered by radial fins
Dp	particle diameter
f	fluid
fin	fin
p	peripheral fin, particle
r	radial fin
s	solid
tip	fin tip

2. One-dimensional heat transfer analysis

The peripheral fin geometry, as displayed in Fig. 1, features hexagonal arrangements of open–pore cells formed by peripheral fins which circumferentially connect radial fins (see Table 1). Specifically, this structure is composed of three distinct levels of fin arrangements, each characterized by the length of radial fin extending from the base tube. The radial lengths in Fig. 1 are 7 mm, 11 mm, and 13.9 mm. All radial and peripheral fins are rectangular in cross section, and have base-line values of widths 4 mm (in the axial direction), and thicknesses 0.25 mm. The radial length, fin width, and fin thickness are also depicted in Fig. 2. The fin width is also called fin pitch.

Table 1
Geometric dimensions of the peripheral fin heat exchanger (unit: m)

D_i	D_o	D_c	P_f	$P_{t,x}$	$P_{t,y}$	δ_t	δ_f
0.004	0.005	0.0055	0.0072	0.0247	0.0286	0.0005	0.00025

Denoting the levels with radial fin lengths of 7 mm, 11 mm, and 13.9 mm to be level 1 (L1), level 2 (L2), and level 3 (L3), respectively, the peripheral fin geometry stacks levels have the following patterns: L3–L1–L2–L1–L2–L1–L3, or L3–L2–L1–L2–L1–L2–L3. Furthermore, each level is staggered with a 30° offset from its neighboring level. As Fig. 3 illustrates the unit cell is defined according to the repetition (periodicity) patterns of levels.

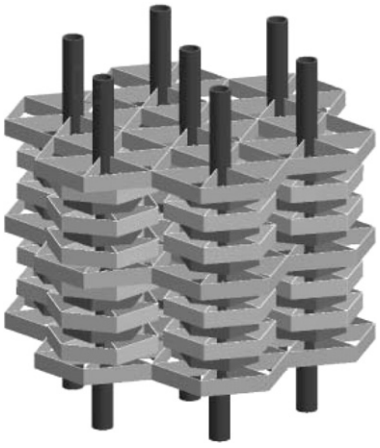

Fig. 1. Peripheral fin heat exchanger.

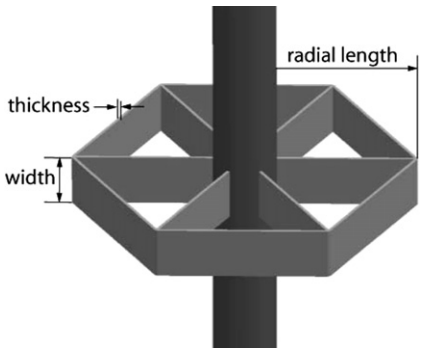

Fig. 2. Description of dimensions.

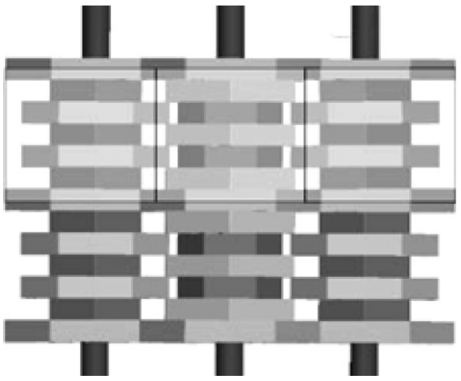

Fig. 3. Unit cells of peripheral fin geometry.

2.1. One-dimensional fin analysis

An energy balance between surface-convection and conduction is applied at the radial fin tip. This would determine the radial fin tip (which is the base of peripheral fin) temperature and heat transfer rates of both fins. The solution described below considered a unit cell under steady-state condition, and assumes negligible radiation heat transfer.

Treating the fin-tube surfaces areas as the interstices of random porous medium, we use the Whitaker particle diameter D_p and Nusselt number Nu_{Dp} correlation [11]. This uses porosity (fraction of volume occupied by air) and an average treatment of surface-convection heat transfer ability based on compiled experiments for various particle shapes and sizes.

The particle diameter is represents the average characteristic length of the fins and is defined based on the interstitial area A per unit solid volume V_s as

$$D_p = \frac{6\,V_s}{A}. \tag{1}$$

Based on this particle diameter, the average Nusselt number for porous media interstitial surface area is

$$Nu_{Dp} = 2 + (0.4Re_{Dp}^{1/2} + 0.2Re_{Dp}^{2/3})Pr^{0.4}, \tag{2}$$

where Pr is the Prandtl number and Re_{Dp} the Reynolds number based on the particle diameter, i.e.,

$$Re_{Dp} = \frac{U_f D_p}{v_f(1-\varepsilon)}, \tag{3}$$

where U_f is the fluid velocity, v_f the fluid kinematic viscosity, and ε the porosity defined as the ratio of fluid volume to total volume

$$\varepsilon = \frac{(1-V_s)}{V}. \tag{4}$$

The surface-convection heat transfer resistance $R_{r(p)}$ is determined as

$$R_{r(p)} = \frac{D_p}{A_{r(p)}Nu_{Dp}k_f}, \tag{5}$$

where k_f is the fluid thermal conductivity, and $A_{r(p)}$ is the total surface-convection are for the perspective fin.

The temperature distribution and the fin heat transfer rate are calculated using the one-dimensional heat flow model. The fin heat transfer rate, Q_{fin}, is [16]

$$Q_{fin} = -k_s A_{k,r}\frac{d\theta}{dx} \text{ at fin base,} \tag{6}$$

where k_s is the thermal conductivity of the solid-conduction, and θ is the fin excess temperature relative fluid, i.e., $\theta = T - T_f$. The distribution for θ is

$$\theta(x) = \theta_b \frac{(\theta_{tip}/\theta_b)\sinh m_{r(p)}x + \sinh m_{r(p)}(L_{r(p)} - x)}{\sinh m_{r(p)}L_{r(p)}}, \tag{7}$$

where $m_{r(p)}$ is the ratio of the solid-conduction to surface-convection resistances for the radial or peripheral fin calculated by Eq. (8), and θ_b is the excess temperature at the tube base, $\theta_b = T_b - T_f$. The expression for $m_{r(p)}$ is

$$m_{r(p)} = \left(\frac{P_{r(p)}}{k_s A_{k,r(p)}A_{r(p)}R_{r(p)}}\right)^{1/2}. \tag{8}$$

Next, using symmetry at mid-plane of the peripheral fins (shown in Fig. 4), the adiabatic tip condition is used.

Then, the fin heat transfer rate Q_f with an adiabatic fin tip is set equal to the Q_f determined by Eq. (6), and this gives

$$\begin{aligned} Q_f &= 2M_p \tanh mL \\ &= -k_s A_{k,r}\theta_b\left[\frac{(\theta_{tip}/\theta_b)\sinh mx + \sinh m(L-x)}{\sinh mL}\right]', \end{aligned} \tag{9}$$

where prime indicates spatial derivative evaluated at the tip of the radial fin, and

$$M_{r(p)} = \left(\frac{P_{r(p)}k_s A_{k,r}\theta_b^2}{A_{r(p)}R_{r(p)}}\right)^{1/2}. \tag{10}$$

Using the above expression, the tip excess temperature θ_{tip} is determined and is then used to determine the fin heat transfer rate from the base of the radial fin, i.e.,

$$Q_f = M_r\frac{(\cosh m_r L_r - \theta_{tip}/\theta_b)}{\sinh m_r L_r}. \tag{11}$$

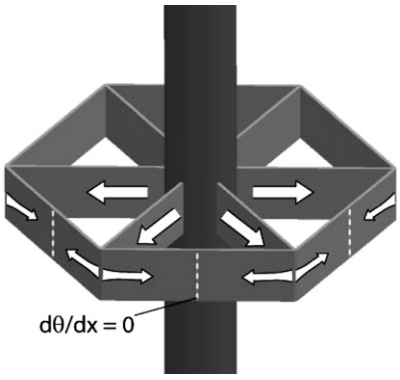

Fig. 4. Adiabatic tip condition used for the location halfway along a peripheral.

From the excess tip temperature θ_{tip}, the actual tip temperature is

$$T = \theta_{tip} + T_f. \quad (12)$$

In addition to the fin heat transfer, the surface-convection heat transfer from the bare area of the tubes is also evaluated using

$$Q_{bare} = (T_b - T_f) Nu_{Dp} \frac{k_s}{D_p} A_{bare}, \quad (13)$$

where A_{bare} is the surface area of the tube not covered by the radial fins.

2.2. Effect of radial fin length on fin heat transfer

Fig. 5 shows that as the radial fin length L_r decreases, the normalized heat transfer rate for a single fin, Q/L_rP_f, increases, indicating an increase of heat transfer rate per unit surface area or unit volume occupied by the fins. Furthermore, decreasing the fin radial length has a larger effect in increasing heat transfer rate, at relatively smaller radial lengths. The radial fin length, however, should have a lower limit from the manufacturing and the condensate hold up (capillarity) considerations.

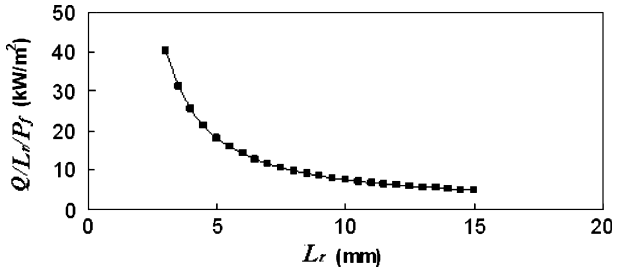

Fig. 5. Decrease in fin length increases normalized heat transfer rate.

3. CFD analysis

3.1. Computational domain and boundary conditions

Fig. 6a shows the computational domain, a three-dimensional representative unit cell, which is composed of six fin levels. Fluid–solid conjugated heat transfer was modeled. There is a fin collar surrounding the tube. Both tube and fin are made of aluminum. The air flow inlet is located 35 mm upstream of the tube center of the front tube row, and the outlet is located 125 mm downstream of the tube center of the last tube row. Uniform air velocity and temperature profiles were applied at the air flow inlet. Zero relative pressure was applied at the outlet.

In the span-wise direction (y axis), symmetry boundary conditions were applied. In the tube axial direction (x axis), periodic boundary conditions were applied at the above and below, as indicated in Fig. 6b. At the tube-side wall boundaries, surface-convection heat transfer boundary condition was applied. Constant tube-side water temperature was applied (average between the tube-side inlet and

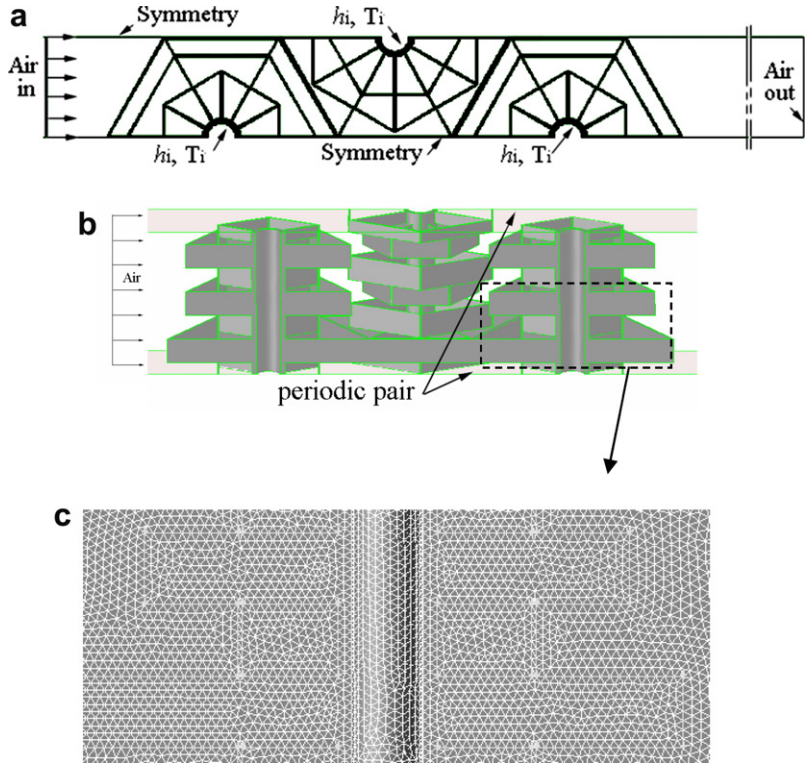

Fig. 6. Sketch-map of computation domain and grids: (a) Computational domain (top view). (b) Fin stacks (color). (c) Typical meshes of fin region in the symmetry plane.

outlet fluid temperatures). The tube-side heat transfer coefficient was calculated by applying the Gnielinski correlation [12]. To compare with conventional plate-fin designs, the boundary conditions are set according to the experimental data of a commercially available plate louver-fin heat exchanger [13]. The air inlet velocity is 1 m/s, inlet temperature is 299.8 K, and the tube-side water average temperature is 324.6 K. The tube-side heat transfer coefficient is 9042 W/(m^2 K).

Unstructured tetrahedral grid was applied. Typical meshes at the symmetric plane are shown in Fig. 6c. For regions near the fin surface and fin collar, the grid had a grid interval size of about the fin thickness, and for the regions away from the fin surface, and the average grid interval size was about 0.15 mm. The number of computational elements is about 2.8 M.

3.2. Numerical method

Our numerical simulation uses CFD [Fluent (Version 6.2)] based on control-volume method [14] applied to the Navier–Stokes and energy equations. Node-based derivative evaluation was used to discretize the convection and diffusion terms of the governing equations (second-order accuracy). The value of the variables at the interface of adjacent cells for the convection terms was interpolated using a second-order upwind scheme. The diffusion terms were central-differenced having second-order accuracy. Pressure–velocity coupling was obtained by SIMPLEC algorithm. W-cycle algebraic multi-grid method with one pre-relaxation sweep was applied to improve the convergence. The convergence criteria required the scaled residuals R^{ϕ} [14] of 10^{-3} for the continuity and momentum equations and 10^{-8} for the energy equation. To ensure the balance of energy, the integrated heat flux from the tube-side was verified to be equal to that from the air-side heat transfer surface and also to that by air flow through the heat exchanger. Temperature-dependent thermophysical properties for air were used.

4. Results and optimization

4.1. Flow and heat transfer characteristics

Fig. 7a shows the top view of the streamlines released from the air inlet. The air impinges on the front surface of the peripheral fins. Most of the entering air flow is deflected by the peripheral fins, while a small portion flows through the narrow gaps between them and enters the inner region. However, the flow in the inner region is relatively stagnant. Therefore, the peripheral fins separate the stronger outside flow from the weaker inner flow.

In the inner region upstream of the tubes, the air flowing through the gaps mainly has a z-direction (Fig. 7a) momentum, which results in a sweep up/down of the adjacent fin surfaces. This shows active mixing which contributes to convection heat transfer of the fin surfaces in the inner region.

The air flow passing the 1st and 2nd tube rows are affected by the next row, and flow pattern for these rows shows somewhat periodic feature. For the 3rd tube row, being the last row, the air flows straight forward from the openings between fins. The downstream streamlines show further converging pattern when we use radial fins with smaller length or peripheral fins are orientated along the span-wise direction.

Fig. 7b shows the velocity vector map in the symmetric plane. The fin geometry is also presented. Strong flows are observed in the outer region of the peripheral fin level-2 and level-1, indicating that the openings in such fin levels are the main flow passage. The flow in the inner region surrounded by the peripheral fins is partly entrained by the main outer region flow.

Intensive surface-convection heat transfer occurs on the periphery fins, especially at the upstream stagnation regions. This is due to the flow impingement and acceleration. Weaker heat transfer is observed behind the tubes where the flow is rather stagnant. Accordingly, the radial fin temperature distribution shows orientation dependence, with larger temperature gradients upstream and smaller gradients downstream, as shown in Fig. 8.

4.2. Influence of condensate/frost blockage

To investigate the condensate/frost blockage formed on the tubes, we place a solid blockage zone around each tube. The blockage-air interface has an elliptic cross section with the center offset slightly downstream (Fig. 9). The thermophysical properties of the blockage zone was specified as frost, with values given in [15], i.e., density of 85 kg/m^3, and thermal conductivity of 0.07 W/(m K). With the frost blockage, the heat transfer rate of the heat exchanger unit cell decreased by 1.7% at an air inlet velocity of 1 m/s, and the pressure drop increased by about 3%. The CFD results show similar flow pattern and heat transfer behavior as those without the blockage. It indicates that the blockage effects of the frost is rather weak, because the region around the tube is rather stagnant. In such cases, the convective heat transfer from the periphery fins is dominant, and the conduction heat transfer through the radial fins is the main path for heat flow to the tubes. So blockage surrounding the tube does not deteriorate the heat transfer and pressure drop performance significantly, compared to the conventional plate-fin heat exchangers.

In practice, frost formation may occur on the front surface of the heat exchanger, because of the higher humidity in air entering there, although the solid temperature is not the lowest there. When that happens, then frost grows in the gap between adjacent peripheral fin levels and blocks the air flow from entering the inner region surrounded by the peripheral fins. However, as mentioned in Section 4.1, the inner region is relatively stagnant even without such blockage. So, any blockage within the gap between

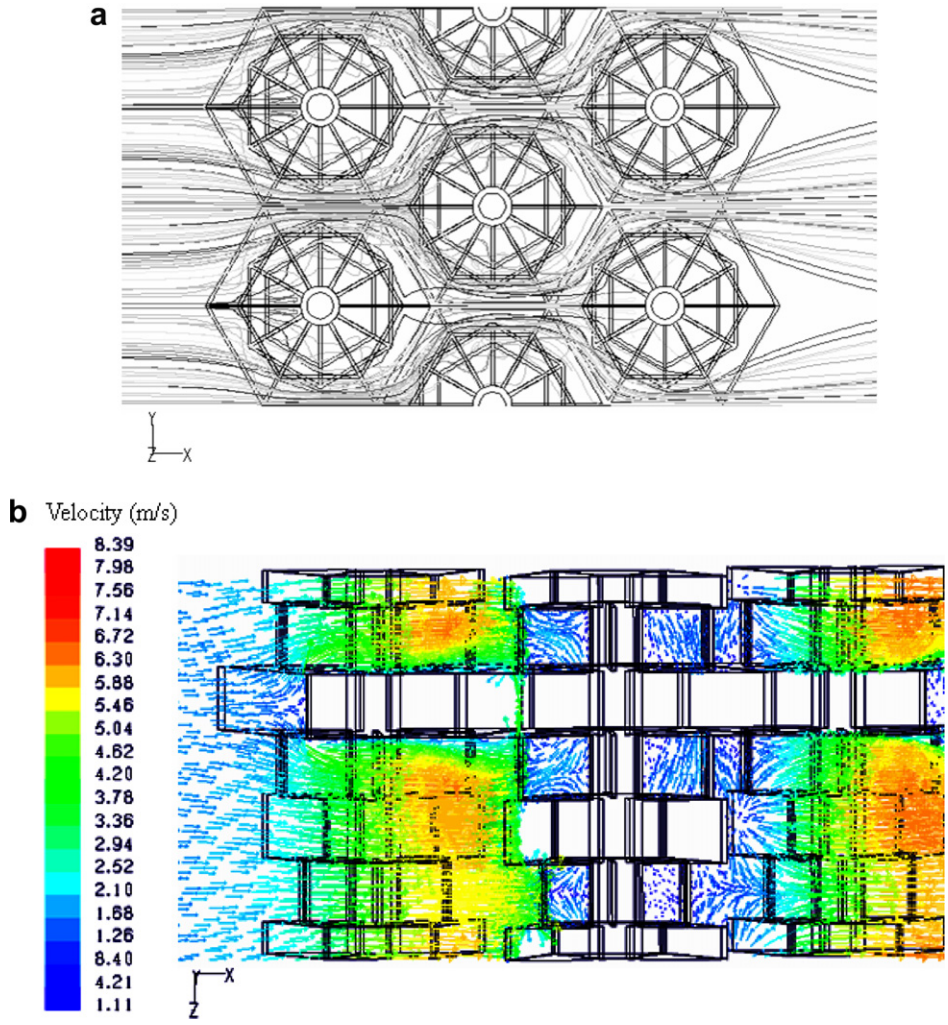

Fig. 7. Flow pattern in the fin region: (a) Top view of streamlines release from air inlet. (b) Side view of velocity vector map in the symmetry plane (color).

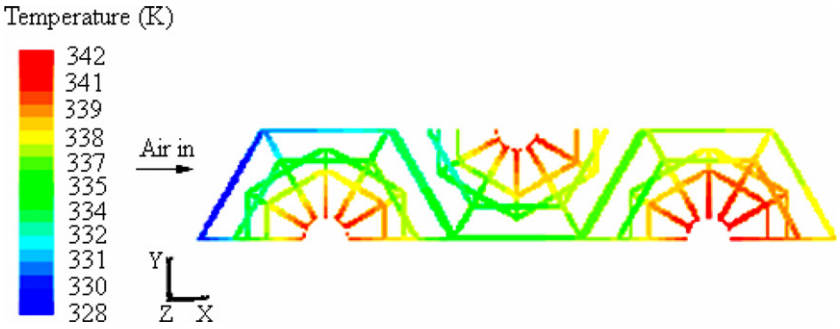

Fig. 8. Contours of constant fin temperature lines (color).

peripheral fin levels at the front surface of the heat exchanger should cause minor effect on the flow and heat transfer behavior. This further indicates potential blockage robustness or frost tolerance characteristic of the peripheral fins.

Although no experimental data is available, when the tube is aligned along gravity, it is expected that the anisotropy of the peripheral fin structure allows for easy drainage of the condensate along the tubes.

4.3. Influence of fin pitch

To study the influence of the fin pitch, another design was simulated using the same boundary conditions and geometrical configuration, except the fin pitch is 4 mm. Comparison of the two fin designs shows that, when the fin pitch changes from 7.2 to 4 mm, the heat transfer rate of the heat exchanger unit cell with the same front surface

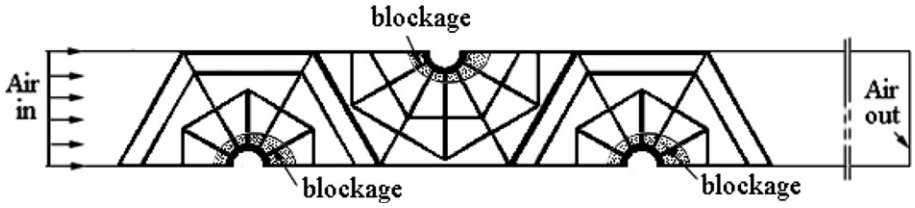

Fig. 9. Sketch-map of computational domain with blockage.

area increases by 10.1%, and the pressure drop of the heat exchanger decreases by 10.2%.

With the smaller fin pitch, the impingement at the peripheral fins is weaker, and the air flow has higher access to the inner region surrounded by the peripheral fins. The air flows through the gaps between adjacent fin levels and the resulting stronger mixing of air flow contributes to the enhanced heat transfer. The weak impingement at the peripheral fins also results in smaller resistance and decreases the pressure drop across the heat exchanger.

However, further decrease in the fin pitch may cause even higher pressure drop, because the friction loss increases with increase in surface area (per unit volume). This may also increase the condensate retention, because of smaller structures (reaching the capillary limit for liquid hold up). So, an optimal fin pitch may exist for peripheral fins.

5. Conclusions

To avoid large pressure drop and heat transfer penalties caused by condensate and frost blockage, an isotropic, peripheral fin structure (connected through radial fins to evaporator tubes) is introduced that allows for alternate fluid flow paths and ease of condensate drainage. The peripheral fins allow for the stagnation–flow region surface convection, while also allowing for sufficient flow interruptions, and these result in both radial and peripheral fins having adequately low surface-convection resistance. The CFD analysis shows the flow in the inner region surrounded by the peripheral fins is relatively stagnant, and the heat transfer at the peripheral fins is dominant (compared to the radial fins). These results also show that the peripheral fins have a blockage robustness advantage.

Acknowledgements

We are thankful to Dr. Steve Wayne of Advanced Heat Transfer LLC and Mr. Olli Naukkarinen of Outokumpu Group for various insights, inputs, and supports.

References

[1] B. Na, R.L. Webb, New model for frost growth rate, Int. J. Heat Mass Transfer 47 (2004) 925–936.
[2] A.F. Emergy, B.L. Siegel, Experimental measurements of the effects of frost formation on heat exchanger performance, in: R.V. Armilli, D.E. Beasley, S. Sengupta (Eds.), Proceedings of AIAA/ASME Thermophysics and Heat Transfer Conference, Heat and Mass Transfer in Frost and Ice packed Beds and Environmental Discharges, HTD-vol. 139, ASME, 1990, pp. 1–7.
[3] J. Yin, A.M. Jacobi, Condensate retention effects on the air-side heat transfer performance of plain and wavy-louvered heat exchangers, Report No. TR-158, University of Illinois at Urbana-Champaign, IL, 2000.
[4] P.W. Eckels, T.J. Rabas, Dehumidification: on the correlation of wet and dry transport processes in plate finned-tube heat exchangers, ASME J. Heat Transfer 109 (1987) 575–582.
[5] C.C. Wang, Y.C. Hsieh, Y.T. Lin, Performance of plate finned tube heat exchangers under dehumidifying conditions, ASME J. Heat Transfer 119 (1997) 109–117.
[6] A.I. Elsherbini, A.M. Jacobi, A model for condensate retention on plain-fin heat exchangers, ASME J. Heat Transfer 128 (2006) 427–433.
[7] A.D. Sommers, A.M. Jacobi, Creating micro-scale surface topology to achieve anisotropic wettability on an aluminum surface, J. Micromech. Microeng. 16 (2006) 1571–1578.
[8] J. Shin, S. Ha, The effect of hydrophilicity on condensation over various types of fin-and-tube heat exchangers, Int. J. Refrig. 25 (2002) 688–694.
[9] J. Kim, M. Kaviany, Purging of dropwise condensate by electrowetting, J. Appl. Phys., submitted for publication.
[10] M. Kaviany, Provisional Patent Application, UMJ-184-A (UM 3251), Robust heat exchanger under condensate and frosting conditions, 2006.
[11] M. Kaviany, Principles of heat transfer in porous media, second ed., Springer, New York, 1995.
[12] S. Kakac, R.K. Shah, W. Aung, Handbook of Single-phase Convective Heat Transfer, John Wiley & Sons, 1987.
[13] H.L. Wu, Y. Gong, X. Zhu, Aspects of flow and heat transfer in louver-fin round-tube heat exchangers, in: Proceedings of 2005 ASME Summer Heat Transfer Conference, No. 72219, July 17–22, San Francisco, California, US, 2005.
[14] Fluent Inc., Fluent 6 User Guide Manual, Lebanon, 2004.
[15] J. Shin, A.V. Tikhonov, C. Kim, Experimental study on frost structure on surfaces with different hydrophilicity: density and thermal conductivity, ASME J. Heat Transfer 125 (2003) 84–94.
[16] M. Kaviany, Principles of Heat Transfer, Wiley, New York, 2001.